Inorganic Chemistry

Communication

pubs.acs.org/IC

Fe_4 Cluster and a Buckled Macrocycle Complex from the Reduction of $[(dmgBF_2)_2Fe(L)_2]$ (L = MeCN, $^tBu^iNC$)

Michael J. Rose, Jay R. Winkler, and Harry B. Gray*

Beckman Institute, California Institute of Technology, Pasadena, California 91125, United States

Supporting Information

ABSTRACT: We report the syntheses, X-ray structures, and reductive electrochemistry of the Fe^{II} complexes $[(dmgBF_2)_2Fe(MeCN)_2]$ (**1**; dmg = dimethylglyoxime, MeCN = acetonitrile) and $[(dmgBF_2)Fe(^tBu^iNC)_2]$ (**2**; $^tBu^iNC$ = *tert*-butylisocyanide). The reaction of **1** with Na/Hg amalgam led to isolation and the X-ray structure of $[(dmgBF_2)_2Fe(glyIm)]$ (**3**; glyIm = glyimine), wherein the $(dmgBF_2)_2$ macrocyclic frame is bent to accommodate the binding of a bidentate apical ligand. We also report the X-ray structure of a rare mixed-valence Fe_4 cluster with supporting dmg-type ligands. In the structure of $[(dmg_2BF_2)_3Fe_3(^1/_2dmg)_3Fe(O)_6]$ (**4**), the $(dmgBF_2)_2$ macrocycle has been cleaved, eliminating BF_2 groups. Density functional theory calculations and electron paramagnetic resonance data are in accordance with a central Fe^{III} ion surrounded by three formally $Fe^{II}dmg_2BF_2$ units.

There has been much interest recently in the mechanism of electrocatalytic dihydrogen (H_2) evolution from acidic solutions containing cobalt diglyoximes.[1−7] Much of this research has been driven by the observation that complexes of the type $[(dmgY)_2Co(L)_2]$ (Y = H, BF_2; dmg = dimethylglyoxime) catalyze the evolution of H_2 under both stoichiometric[1] and electrocatalytic[2,3] reaction conditions. Chao and Espenson studied the mechanism of H_2 formation from $[(dmgH)_2Co(L)]$ (L = PR_3, py, Cl^-),[1] and we and others have reported related work on the fluoroborated $[(dmgBF_2)_2Co(MeCN)_2]$ (MeCN = acetonitrile).[3,4] H_2 generation has also been achieved on catalyst-modified glassy carbon electrodes by Berben and Peters.[5] Fontecave et al.[6] and Eisenberg et al.[7] have utilized cobalt catalysts with photosensitizers, thus enabling the photocatalytic generation of H_2. Recent work by Chang and coworkers reflects the utility of polypyridine ligands in supporting cobalt-based electrocatalysis in aqueous solutions,[8] and biomimetic iron catalysts have also shown promise as hydrogen-generating electrocatalysts.[9]

We have begun a program to study catalytic reductions involving diglyoximatoiron(II) species analogous to those reported by Pang and Stynes.[10−14] The complexes are macrocyclic species bearing two glyoximato ligands linked by difluoroboronyl (BF_2) or diphenylboronyl (BPh_2) groups. The $Fe^{III/II}$ reduction potentials depend on the axial ligand, ranging from +0.406 V (L = MeIm; linker = BF_2) to +1.16 V vs SCE (L = *p*-toluenesulfonylmethyl isocyanide, BF_2).[11] The electrochemistry of several tetraimine iron systems at negative potentials has been investigated, as in the cases of Me_6[14]-1,3,8,10-cyclotetradecane-N_4-tetraene (tetraeneN_4) and 2,3,9,10-Me_4-1,4,8,11-N_4-cyclotetradecanetetraene (tim) iron complexes.[15,16] Indeed, the reduction of $[(tim)Fe(MeCN)_2]^{2+}$ led to isolation of an unexpected Fe^I–Fe^I dimer, $[\{(tim)Fe\}_2]$, which was structurally characterized.[17] However, no such study has been reported for a glyoxime-based ligand system.

In this work, we have structurally characterized several $[(dmgBF_2)_2Fe^{II}(L)_2]$ species derived from the $dmgBF_2$ macrocycle [L = MeCN, $^tBu^iNC$ (*tert*-butylisocyanide)]. In addition to determining the potentials for these systems, we show that the reduction of $[(dmgBF_2)_2Fe(MeCN)_2]$ with Na leads to the formation of a Fe_4dmg cluster $[(dmg_2BF_2)_3Fe_3(^1/_2dmg)_3Fe(O)_6]$, wherein the ligand frame has been partially reduced. Under slightly different conditions, reduction leads to the formation of a "buckled macrocycle" stucture, in which the $(dmgBF_2)_2$ macrocycle is distorted from the equatorial plane of the Fe^{II} center to accommodate an apical, bidentate glyimine ligand.

The species $[(dmgBF_2)Fe^{II}(MeCN)_2]$ (**1**) was synthesized according to a published procedure.[10,11] Slow evaporation of **1** in $CHCl_3$/MeCN (5:1) afforded light-orange blocks suitable for X-ray diffraction. The overall structure is octahedral, with the macrocyclic $(dmgBF_2)_2$ ligand occupying the four equatorial sites, as found in all FedmgBF_2 complexes, with two MeCN ligands in the axial coordination sites. The Fe–N_{dmg} bond distances in **1** [1.8918(5) Å] are similar to those for $[(dmgBPh_2)_2Fe^{II}(MeCN)_2]$ [Fe–N_{dmg} = 1.898(8) Å],[21] in which the two BF_2 linkers are substituted for BPh_2. The Fe–N_{MeCN} bond distance in **1** [1.9387(4) Å] also is similar to that found in the BPh_2-linked complex mentioned above (Fe–N_{MeCN} = 1.941 Å).[18]

The addition of 2 equiv of $^tBu^iNC$ in MeCN affords the bis(isocyanide) complex $[(dmgBF_2)Fe(^tBu^iNC)_2]$ (**2**) in good yield. Slow evaporation of MeCN/toluene afforded dark-orange blocks of **2** (structure shown in Figure 1). The Fe–N distances in **2** [Fe–N = 1.8905(7) and 1.8886(7) Å] are similar to those in **1**, while the axial Fe–C bonds [Fe–C = 1.9064(9) Å] are shorter than the Fe–N_{MeCN} distances in **1** [1.9387(4) Å], likely attributable to back-bonding from Fe^{II} to the isocyanides. The isocyanides are farther from the Fe center compared to the carbonyl complex $[(dmgBF_2)Fe(CO)(py)]$ [Fe–CO = 1.772(6) Å],[14] consistent with the greater back-bonding ability of CO.

Received: October 19, 2011
Published: February 9, 2012

   dx.doi.org/10.1021/ic202253v | *Inorg. Chem.* 2012, 51, 1980–1982

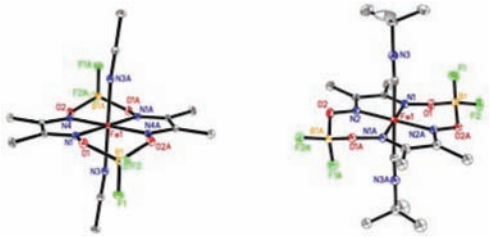

Figure 1. ORTEP diagrams (50% ellipsoids) of **1** (left) and **2** (right). Selected bond distances (Å) and angles (deg) for **1**: Fe−N_{dmg} = 1.8918(5), Fe−N_{MeCN} = 1.9387(4); N_{MeCN}−Fe−N_{MeCN} = 180.0. For **2**: Fe−$N1_{dmg}$ = 1.8905(7), Fe−$N2_{dmg}$ = 1.886(7), Fe−C = 1.9064(9); C−Fe−C = 180.0.

The cyclic voltammogram (CV) of **1** exhibits a two-electron reductive wave near −1.75 V vs SCE (see Supporting Information, Figure S1). The reduction potential of **1** is much more negative than that of $[(dmgBF_2)_2Co(MeCN)_2]$ (−0.55 V) or [(dmgH)Ni] (−1.05 V). The formation of $Fe^{I/0}$ or ligand-reduced species is equally plausible. Substitution of MeCN (**1**) for $^tBu^tNC$ (**2**) results in a small shift of E_{red} to −1.65 V (see the Supporting Information, Figure S2). The negative potentials exhibited by **1** and **2** prompted us to use a strong chemical reductant in an attempt to isolate a reduced species. The reaction of an orange slurry of **1** in MeCN/tetrahydrofuran (THF) (1:1) with 2 equiv of Na/Hg amalgam led to the formation of a dark-red solution. Filtration and crystallization [MeCN−THF/diethyl ether (Et_2O)] under an inert atmosphere afforded small crystals suitable for synchrotron X-ray diffraction. The resulting structure reveals a strained binding motif of the $(dmgBF_2)_2$ macrocycle (Figure 2, left),

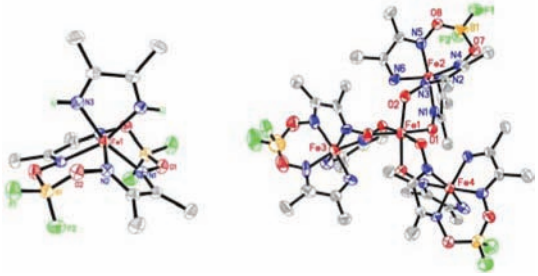

Figure 2. ORTEP diagrams (50% ellipsoids) of **3** (left) and **4** (right). Selected bond distances (Å) and angles (deg): Fe−$N1_{dmg}$ = 1.925(2), Fe−$N2_{dmg}$ = 1.886(2), Fe−$N_{N_2H_2}$ = 1.916(2); $N_{N_2H_2}$−Fe−$N_{N_2H_2}$ = 78.50(9). For **4**: Fe−$N1_{dmgBF_2}$ = 1.903(4) and 1.876(9), Fe−$N2_{dmgBF_2}$ = 1.912(5) and 1.91(2), Fe−N_{dmgNOH} = 1.923(6) and 1.92(1), Fe−O = 2.005(4).

wherein the ligand no longer occupies the equatorial coordination sites. Overall, we assign the structure as $[(dmgBF_2)_2Fe(glyIm)]$ (**3**; glyIm = glyimine), which, to our knowledge, represents a novel bonding motif for a $(dmgBF_2)_2$ system (Figure S3).

The imine NH's were identified in the difference map and refined isotropically. The Fe−NH distance [1.916(2) Å] is similar to those observed between the Fe center and glyoximato N donors. Although the $(dmgBF_2)_2$ macrocycle appears strained, each diglyoxime moiety retains planarity; thus, the bending occurs across the $O(BF_2)O$ unit. However, the B-atom pivot retains an sp^3 geometry close to ideal values [103.4(2)−114.6(2)°]; for comparison, the corresponding $O(BF_2)O$ unit in **1** exhibits a similar range of bond angles [104.86(5)−117.34(5)°].

We performed a similar reduction followed by workup under *aerobic* conditions, affording instead a *bright-violet* solution. Subsequent filtration and crystallization (MeCN−THF/Et_2O) afforded dark-violet needles suitable for X-ray analysis. The resulting Fe_4dmg cluster $[(dmg_2BF_2)_3Fe_3(^1/_2dmg)_3Fe(O)_6]$ (**4**; Figure 2, right) in trigonal $R\bar{3}$ consists of a central Fe unit, surrounded by three peripheral Fe ions in dmg_2BF_2-type ligation. This results in 3-fold rotational symmetry, although there is no crystallographic symmetry within the cluster itself.

On the periphery of the cluster, each Fe center is coordinated by a "half-broken" $(dmg)_2BF_2$ half-macrocycle, wherein one fluoroboronyl group and one oximato N−OH unit have been reductively eliminated (presumably forming H_2O). The broken dmg_2BF_2 unit provides one imino N and four oximato N donors to the peripheral octahedral Fe centers. The last two coordination sites of the peripheral Fe atoms are occupied by the two N donors of a "$^1/_2$dmg" moiety. Indeed, $NaBF_4$ (ν_{BF} = 1084 cm^{-1}) is observed as a byproduct (precipitates prior to crystallization). Overall, it appears that the cluster with reduced ligand moieties is more stable than an Fe^I intermediate, in contrast to the metal-centered reduction found in $[(dmgBF_2)_2Co^I(MeCN)_2]^-$.[2,19] The central Fe ion is octahedrally coordinated by oximato O donors from the broken dmg macrocycles. Each oximato O atom is bonded to an oxime N atom that is coordinated to a peripheral Fe atom, forming a tight $\{Fe_{cent}-O-N-Fe_{periph}\}$ interaction, which links the central and peripheral Fe sites just two atoms apart (Fe−Fe distance = 3.84 Å).

The charge balance of the neutral cluster suggests the presence of three formally Fe^{II} centers and one Fe^{III} center. The three peripheral Fe ions are in dmg_2BF_2-type ligation, which stabilizes the Fe^{II} state to a great extent [$E_{1/2}(Fe^{III/II}) \approx +0.850$ V vs SCE], as is also found in other multinuclear complexes, $[(N3)Cr^{III}\{\mu\text{-}(dmg_3)Fe^{II}\}Cr^{III}(N3)]$, for example, where magnetic and electrochemical studies confirmed the Fe^{II} oxidation state.[20] In contrast, the anionic $(O6)^{6-}$ donor set at the central Fe site stabilizes an Fe^{III} center. The X-band electron paramagnetic resonance (EPR) spectrum of **4** in MeCN/toluene (3:1) frozen glass at 77 K (Figure S5) is indicative of a slightly rhombic, low-spin d^5 system, consistent with the assignment of a low-spin Fe^{III} center in $(O6)^{6-}$ coordination at the center of the cluster. Additionally, **4** exhibits μ_{eff} = 1.92 μ_B in the solid state (298 K), in agreement with solution EPR data.

This result is surprising in view of the electronic structures of other octahedral Fe^{III} complexes containing O donors. For example, the {Fe−O6} fragment of $[Fe^{III}(acac)_3]$[21] is structurally similar [Fe−O_{avg} = 1.992(21) Å] to **4** [Fe−O_{avg} = 2.005(4) Å]. However, $[Fe^{III}(acac)_3]$ is high-spin ($S = {}^5/_2$)[22,23] and displays an EPR spectrum in MeCN/toluene frozen glass at 77 K with features near $g \approx 4$ (see the Supporting Information, Figure S5). Another related complex, $[Fe^{III}(ox)_3]^{3-}$ (ox = oxalate), mimics the $(O6)^{6-}$ donor set found in **4** more accurately but also exhibits an $S = {}^5/_2$ ground state that gives rise to features in its EPR spectrum near $g \approx 4$ in frozen solutions (H_2O, 77 K).[24] We conclude that glyoximato O donor ligand-field splitting in **4** is greater than that associated with carboxylato O ligation in $[Fe^{III}(ox)_3]^{3-}$, with the result that **4** in frozen solution adopts a low-spin state.

We undertook density functional theory (DFT) calculations (PW91/6-31G*) to investigate localization of the $S = {}^1/_2$ spin (based on EPR results) on the central {Fe−O6} unit in **4**. The

dx.doi.org/10.1021/ic202253v | *Inorg. Chem.* 2012, 51, 1980−1982

calculated bond distances are generally in good agreement with the X-ray structure (see Supporting Information, Table S2). The resulting spin density (Figure 4, left) is focused at the

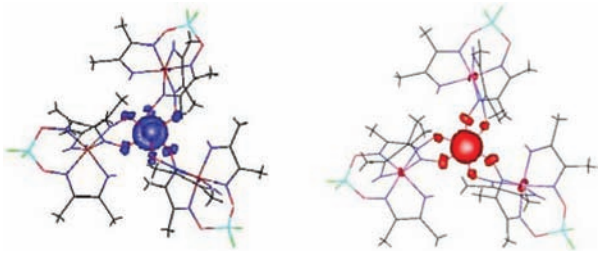

Figure 4. DFT-calculated spin-density plots of **4** optimized at $S = {}^{1}/_{2}$ (left) and ${}^{5}/_{2}$ (right) configurations.

central Fe site (78.1%) versus the peripheral Fe sites (<3.5%). We found that the spin and population densities were largely independent of the chosen basis set or functional (see the Supporting Information, Table S5). This suggests that the central Fe alone exhibits the higher (Fe^{III}) oxidation state.

We now consider the Fe−O bond distances, which are much longer (~0.07 Å) in the crystal structure (~2.01 Å) than in the $S = {}^{1}/_{2}$ calculated values (PW91/6-31G*, 1.93 Å; PW91/TZP, 1.95 Å; see Supporting Information, Table S2), strongly suggesting partial population of a *high-spin* Fe^{III} center in the solid state at 100 K. We performed a DFT calculation assuming an $S = {}^{5}/_{2}$ ground state, which more accurately reproduced the crystallographically determined bond distances in the central {Fe−O6} unit ($Fe-O_{calc}$ = 2.02 Å; $Fe-O_{expt}$ = 2.01 Å). Additionally, we found the geometry-optimized $S = {}^{5}/_{2}$ configuration to be ~9.1 kcal/mol more stable than the geometry-optimized $S = {}^{1}/_{2}$ configuration. In the $S = {}^{5}/_{2}$ configuration, the spin density also remained localized at the central Fe^{III}(O6) moiety (87%), with only ~1% spin density at each peripheral Fe^{II} site (Figure 4, right side). We conclude that there must be a high-spin/low-spin equilibrium, with population of the low-spin complex in glassy solutions at low temperatures. We plan to report a more complete description of this spin-equilibrium system from variable-temperature structural data in combination with the results from Mössbauer and temperature-dependent magnetic susceptibility experiments.

■ ASSOCIATED CONTENT

Ⓢ Supporting Information

CIF files for **1**−**4**, crystal data for **1**−**4** (Table S1), bond distances and angles for **1**−**4** (Table S2), DFT parameters (Tables S3 and S4), spin densities of **4** (Table S5), CVs of **1** and **2** (Figures S1 and S2), additional ORTEP views of **3** and **4** (Figures S3 and S4), EPR spectra (Figure S5), and UV/vis absorption spectrum of **4** (Figure S6). This material is available free of charge via the Internet at http://pubs.acs.org.

■ AUTHOR INFORMATION

Corresponding Author

*E-mail: hbgray@caltech.edu.

Author Contributions

All authors have given approval to the final version of the manuscript.

Notes

The authors declare no competing financial interest.

■ ACKNOWLEDGMENTS

The authors thank Larry Henling and Michael Day for X-ray structures and Angelo Di Bilio for assistance with EPR spectra. We acknowledge Allen Oliver (University of Notre Dame) and Jeannette Krause (University of Cincinati) for X-ray data collection on **3** via the *SCrALS* program at Beamline 11.3.1, Advanced Light Source (LBNL), supported by the U.S. DOE, Energy Material Sciences Division. The Bruker KAPPA APEX II was purchased via an NSF CRIF:MU. The authors thank Nicole Fry for obtaining magnetic susceptibility data on **4**. Funding sources: NSF Grant CHE-0802907 (to M.J.R., J.R.W., and H.B.G.); NSF Grant CHE-1042009 (to M.J.R.); Grant DOE-AC02-05CH11231 (synchrotron X-ray structure); NSF Grant CHE-0639094 (Mo Kα X-ray structures).

■ REFERENCES

(1) Chao, T.-H.; Espenson, J. H. *J. Am. Chem. Soc.* **1978**, *100*, 129−133.
(2) Hu, X.; Brunschwig, B. S.; Peters, J. C. *J. Am. Chem. Soc.* **2007**, *129*, 8988−8998.
(3) Baffert, C.; Artero, V.; Fontecave, M. *Inorg. Chem.* **2007**, *46*, 1817−1824.
(4) Dempsey, J. R.; Winkler, J. R.; Gray, H. B. *J. Am. Chem. Soc.* **2010**, *132*, 1060−1065.
(5) Berben, L. A.; Peters, J. C. *Chem. Commun.* **2010**, 398−400.
(6) Fihri, A.; Artero, V.; Razavet, M.; Baffert, C.; Leibl, W.; Fontecave, M. *Angew. Chem.* **2008**, *47*, 564−567.
(7) Du, P.; Schneider, J.; Luo, G.; Brennessel, W. W.; Eisenberg, R. *Inorg. Chem.* **2009**, *48*, 4952−4962.
(8) Sun, Y.; Bigi, J. P.; Piro, N. A.; Tang, M. L.; Long, J. R.; Chang, C. J. *J. Am. Chem. Soc.* **2011**, *133*, 9212.
(9) Tye, J. W.; Lee, J.; Wang, H.-W.; Mejia-Rodriguez, R.; Reibenspies, J. H.; Hall, M. B.; Darensbourg, M. Y. *Inorg. Chem.* **2005**, *44*, 5550−5552.
(10) Pang, I. W.; Stynes, D. V. *Inorg. Chem.* **1977**, *16*, 590−594.
(11) Thompson, D. W.; Stynes, D. V. *Inorg. Chem.* **1990**, *29*, 3815−3822.
(12) Hess, C. R.; Weyhermüller, T.; Bill, E.; Wieghardt, K. *Angew. Chem., Int. Ed.* **2009**, *48*, 3703−3706.
(13) Thompson, D. W.; Stynes, D. V. *Inorg. Chem.* **1991**, *30*, 636−640.
(14) Harshani de Silva, D. G. A.; Leznoff, D. B.; Impey, G.; Vernik, I.; Jin, Z.; Stynes, D. V. *Inorg. Chem.* **1995**, *34*, 4015−4025.
(15) Rakowski, M. C.; Busch, D. H. *J. Am. Chem. Soc.* **1975**, *97*, 2570.
(16) Norman, J. G. J.; Chen, L. M.; Perkins, C. M.; Rose, N. J. *Inorg. Chem.* **1981**, *20*, 1403.
(17) Hess, C. R.; Weyhermüller, T.; Bill, E.; Wieghardt, K. *Angew. Chem., Int. Ed.* **2009**, *48*, 3703−3706.
(18) Vernik, I.; Stynes, D. V. *Inorg. Chem.* **1996**, *35*, 6210.
(19) Shi, S.; Daniels, L. M.; Espenson, J. H. *Inorg. Chem.* **1991**, *30*, 3407−3410.
(20) Burdinski, D.; Birkelbach, F.; Weyhermüller, T.; Flörke, U.; Haupt, H.-J.; Lengen, M.; Trautwein, A. X.; Bill, E.; Wieghardt, K.; Chaudhuri, P. *Inorg. Chem.* **1998**, *37*, 1009−1020.
(21) Roof, R. B. *Acta Crystallogr.* **1956**, *9*, 781−786.
(22) Gerloch, M.; Lewis, R. C. *J. Chem. Soc. A* **1969**, 1422−1427.
(23) Hedewy, S.; Hoffman, S. K. *Phys. Status Solidi A* **1986**, *97*, 129−133.
(24) Collison, D.; Powell, A. K. *Inorg. Chem.* **1990**, *29*, 4735.